NJC

Cite this: *New J. Chem.*, 2012, **36**, 2184–2187

www.rsc.org/njc

LETTER

Aerosol copper initiated core–shell nanoparticle synthesis and micropatterning

Jeong Hoon Byeon[a] and Young-Woo Kim*[b]

Received (in Montpellier, France) 28th June 2012, Accepted 27th August 2012
DOI: 10.1039/c2nj40553a

We report the development of copper–silver core–shell nanoparticles where the aerosol copper nanoparticles served as the seeds for the deposition of silver atoms on their surface. The copper particles were also electrostatically patterned on the substrate to fabricate silver micropatterns.

Metal nanoparticles are probably the most extensively researched nanomaterials and a frequent tool in nanotechnology. The development of synthetic routes for desired single and binary metal nanomaterials has been a great major task for both theoretical and practical applications.[1] Bimetallic nanoparticles have excellent optical, electronic, and catalytic properties different from those of their component metals.[2] Therefore, much attention has been received by the development of applications such as catalysts, electronic devices, and substrates for surface-enhanced Raman scattering.[3] Among many bimetallic nanoparticles, the copper–silver bimetallic system has recently received much attention due to its high electron conductivity and application as a lead-free solder alloy.[4]

There have been extensive efforts focusing on the development of new synthetic methodologies for bimetallic nanoparticles with wet chemical or high-vacuum-temperature processes; such methods need either a sophisticated setup or involve difficulty in handling chemicals.[5] Depending on the synthesis procedure, the bimetallic nanoparticles can be synthesized homogeneously with the simultaneous reduction of two metal ions or heterogeneously by successive reduction of two metal ions. More studies are required to develop convenient synthesis methods for copper–silver bimetallic particles.

Despite the existence of many works on bimetallic nanoparticle preparation, there are no reports on aerosol based methods with the characteristics of being simple, low-cost, versatile, and green. In this work, we describe our new strategy regarding the silver overgrowth on preformed aerosol copper nanoparticles by transmetalation,[4] *i.e.* the reduction of silver ions on the surface of preformed copper nanoparticles where the copper is the reducer. Spark generated aerosol copper nanoparticles were used as seeds for the overgrowth of silver deposits in a precursor solution with the presence of ultrasound. The application of ultrasound during the silver deposition process generates a specific agitation due to the mechanical effect (shock wave, dispersion, *etc.*, leading to a good mixing of the chemical species) on the surface of the copper particles in the silver precursor solution, which leads to a faster deposition of silver than conventional mechanical agitation.[6] This method is then applied to site selective deposition of silver from the electrostatically patterned aerosol copper nanoparticles.

The overall steps involving spark copper generation were used to deposit silver on the surface of a copper nanoparticle and they are schematically described in Fig. 1. The method involves the generation of aerosol copper particles *via* a spark discharge[7] and their thermophoretic deposition on a polymer substrate. The spark discharge is a kind of atmospheric-pressure nonequilibrium discharge.[8] While the temperature of the particle-laden flow was kept at 20 °C using a tube heater, the temperature of the polymer substrate was maintained at 5 °C, thereby enhancing the deposition of the particles onto the substrate *via* thermophoresis. Thermophoretic velocities were calculated according to the expression of the particles, with Knudsen's number >3:

$$v_{th} = -\frac{3}{8}\frac{\mu_g \nabla T}{0.499\rho_g T_g(1+\pi\alpha/8)} = -K_{th}\frac{\mu_g \nabla T}{\rho_g T} \qquad (1)$$

where ∇T represents the temperature gradient in the vicinity of the particle, α is the accommodation coefficient, and K_{th} (= 0.54) is the numerical coefficient estimated at α = 1,[9] which increases with decreasing particle size. The thermophoretic velocity ranged from 1.9 to 0.5 m s^{-1} for the particle sizes (*cf.* 0.36 m s^{-1} for flow velocity). Eqn (1) (which has a variation

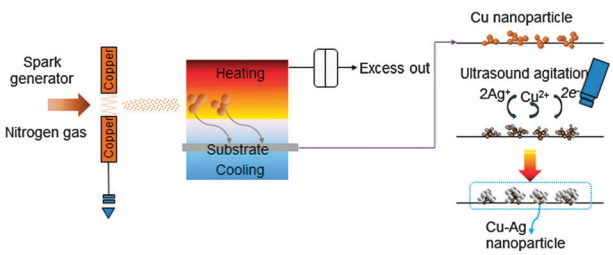

Fig. 1 Schematic diagram of aerosol based fabrication used for this work.

[a] *Department of Chemistry, Purdue University, Indiana 47907, USA*
[b] *Department of Automotive Engineering, Hoseo University, Asan 336-795, Republic of Korea. E-mail: ywkim@hoseo.edu; Fax: +82 41 540 5818; Tel: +82 41 540 5819*

of less than 10% over the velocity distribution) offered a reasonably accurate simple expression for predicting the thermophoretic deposition of particles. The aerosol copper particles acted as seeds and became kinetically capable of reducing the incoming silver ions onto the seed particles to create copper–silver core–shell configurations. The proposed transmetalation reaction is as follows:[2,4]

$$n\mathrm{Cu}^0 + n\mathrm{Ag}^+ \xrightarrow{\mathrm{CH_3CHO}} n\mathrm{Ag}^0 + n'\mathrm{Cu}^0 + n''\mathrm{Cu}^{2+} \qquad (2)$$

During the reaction, silver was deposited through redox chemistry involving the silver ion. n' and n'' mean the remainders of Cu^0 and Cu^{2+}, respectively, because the reduction rate of the silver ion is faster ($Ag^+/Ag^0 = 0.78$ V) than that of Cu^{2+}, so that the reduction of the silver ion is preferred on the copper particles. Silver islands which are formed on the surface of the copper particles in the reaction act as the active sites for the further deposition of silver species.

The size distribution of the copper nanoparticles was measured using a scanning mobility particle sizer (3936, TSI, US), and the result is provided in Fig. 2a. The total number concentration (TNC), geometric mean diameter (GMD), and geometric standard deviation (GSD) of the spark generated copper particles were 1.57×10^7 particles cm^{-3}, 30.9 nm, and 1.52, respectively. The morphology and structure of the particles were characterized by a transmission electron microscope (TEM, 3010, JEOL, Japan) and electron diffraction (ED). For the purposes of characterization, the copper nanoparticles were deposited on a carbon-coated copper grid. The TEM image (Fig. 2b) revealed that the copper particles were agglomerates of several primary particles (each ~3 nm in diameter). Fig. 2b also shows the ED pattern corresponding to the TEM micrograph. The pattern has a sharp diffraction line showing the (111) reflection and weak diffraction lines showing the (200) and (220) reflection of the face-centered cubic lattice for metallic copper, which indicated that the particles grew predominantly along the (111) lattice and mostly consisted of several nanometer sized crystallites. Fig. 2c shows a scanning electron microscope (SEM, JSM-6500F, JEOL) image of the surface of the thermophoretically copper deposited polytetrafluoroethylene (PTFE) substrate. As is seen from the image, the deposition of the copper particles on the substrate was achieved. The following three images show the energy dispersive X-ray (EDX, JED-2300, JEOL, Japan) maps of the SEM image. These maps correspond to carbon, fluorine, and copper, respectively. The dots in these images indicate the existence of each element in the SEM image. It could be suggested that the substrate was deposited with copper particles, whereas carbon and fluorine, which might have originated from the substrate itself, were also detected.

In Fig. 3a, for the initial stage of silver deposition (1.5 min, left images), small particles (~40 nm) formed on the surface of the copper particles. A contrast of the particles shows a character of the core–shell structure. In the process of time, silver particles were continuously grown along with the copper particles, and finally, for the finial state of the deposition (5.0 min, right images), the silver particles became larger (~90 nm). The increase in particle size with increased deposition time (*i.e.* increasing the silver content in the bimetallic particles) can be explained by considering the continuous reduction of silver ions, and thus, there was no contrast, otherwise the initial stage. The copper particles effectively acted as seeds to initiate the silver deposition. The process was hence clearly observed to occur by the initial nucleation at several sites on the copper followed by the diffusion of silver ions toward the growing silver islands and reduction to silver atoms on the copper particles. The deposited silver atoms then acted as a self-catalyst for further silver deposition, and a continuous silver overgrowth on the copper particle was then obtained. Fig. 3b shows the EDX maps for the grown particles. The SEM images and their following maps correspond to copper and silver, and dots and contours (red: silver, green: copper) in these maps indicate the positions of elemental copper and silver in the SEM images, which shows that the silver deposition produced copper–silver core–shell particles. Fig. 3c shows X-ray diffraction (XRD, RINT-2100, Rigaku, Japan)

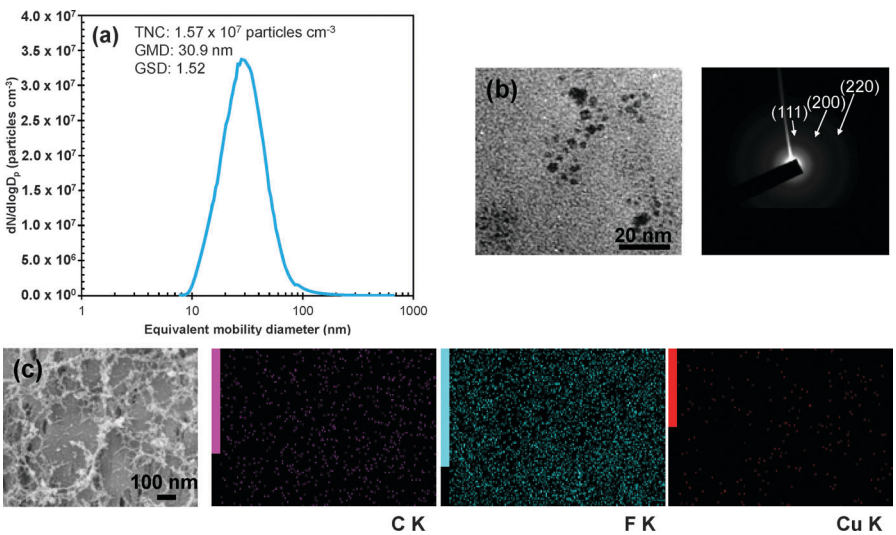

Fig. 2 Results for spark generated copper nanoparticles. (a) Size distribution of the spark produced copper nanoparticles. (b) TEM image for the spark produced copper nanoparticles and its ED pattern. (c) EDX maps of the copper deposited substrate.

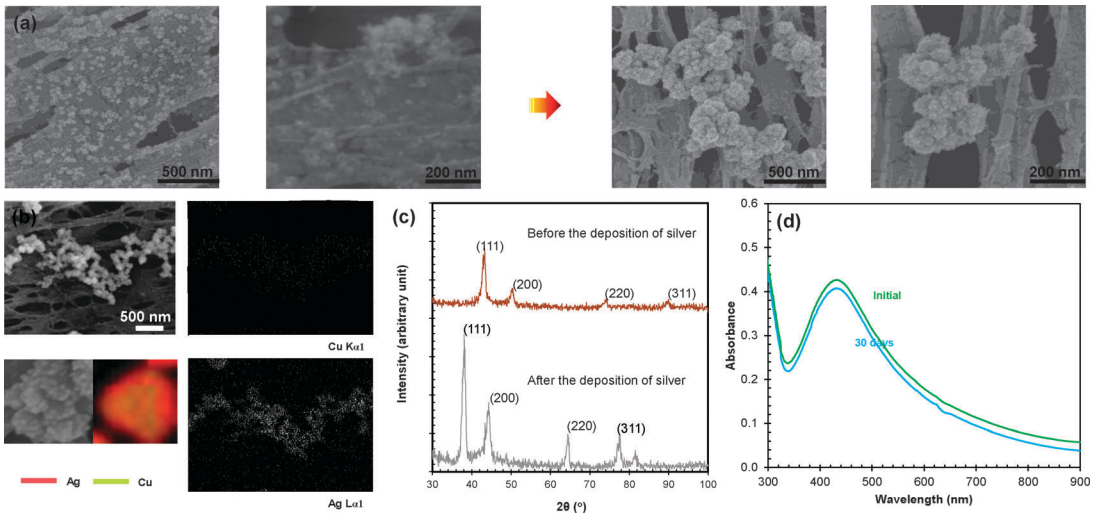

Fig. 3 Results for copper–silver core–shell nanoparticles. (a) SEM images of the core–shell particles with different reaction times. (b) EDX maps of the core–shell particles. (c) XRD diffractograms of particles before and after deposition of the silver. (d) UV-vis spectra of the core–shell particles with different air exposure times.

patterns of the particles before and after deposition of the silver. The peaks for the cases are consistent with elemental copper and silver, respectively. For the after silver deposition, the diffractogram did not show bimodal peaks (only show a slight shifting of the peaks) for each crystal lattice, implying that the seed copper particles were completely covered with thick silver layers. Fig. 3d shows that the UV-vis (330, Perkin-Elmer, US) spectra exhibited peaks at ~435 nm corresponding to the surface plasmon resonance (SPR) absorption of the particles. The absorption peaks shifted (red shift) from ~405 nm (a typical SPR band of pure silver nanoparticles in the 320–500 nm region with a peak at ~405 nm)[10] to ~435 nm (in the 320–800 nm, the present cases). In these cases, where the silver shell is sufficiently thick, the silver SPR peak is mainly observed, demonstrating the relative composition/thickness dependent optical properties.[11] The red shift and broadening of the SPR band in this work were consistent with the fact that the dominant products were copper–silver bimetallic particles. According to the Mie theory, the position of the SPR band maxima of the particles was sensitive to changes in refractive index of the embedding medium in accordance with the following equation,

$$\lambda_{peak}{}^2 = (2\pi c_l)^2 m N e^2 (\varepsilon_\infty + 2n^2)/\varepsilon_0 \qquad (3)$$

where λ_{peak} is the position of the SPR band, c_l is the speed of light, m is the effective mass of conduction electrons, N is the free electron concentration, e is the electronic charge, ε_∞ is the optical dielectric function of the metal, and ε_0 is the free space permeability. The theoretical SPR band is 433 nm, which is consistent with the measured data. Moreover, there are no significant differences between the exposure days. This implies that the core–shell particles had stability since the silver deposit should provide protection to the copper against oxidation.

Fig. 4a schematically shows the processes of micropatterning. Spark generated copper nanoparticles were injected into a deposition chamber with an electric field between the pattern template [*i.e.* copper grids, G100 (2010C-XA), G300 (2030C-XA), and G600 (2060C-XA) square grids, SPI Supplies, US] and ground potential. The predicted value of v_{mig} is determined by balancing the electrostatic force and the Stokes viscous force. For the injected copper particles, the theoretical migration velocity to a substrate takes the following expression:[12]

$$v_{mig} = \frac{q_p E C_c}{3\pi\mu_g D_p} \qquad (4)$$

where q_p is the particle charge, E is the electric field strength, and C_c is the slip correction factor. The mean migration velocity is 1.1 m s^{-1}, which is higher than that of flow velocity (0.4 m s^{-1}). The deposition density of the polymer was selected to be approximately 1.5×10^{-2} mm^2 copper per mm^{-2} of substrate. Fig. 4b shows SEM images, which verify the copper particles only in a line of the pattern. Fig. 4b also shows SEM images of the micropatterns with different pattern sizes after a reaction in the silver precursor solution. As shown in Fig. 4b, the silver deposition occurred on the copper particles, *i.e.* at the copper deposited region of the substrate. The resistivities (ρ) of the patterns without sintering were calculated through the relationship $\rho = RA/L$, where R, A, L are the resistance, cross-sectional area, and length of the pattern, respectively.

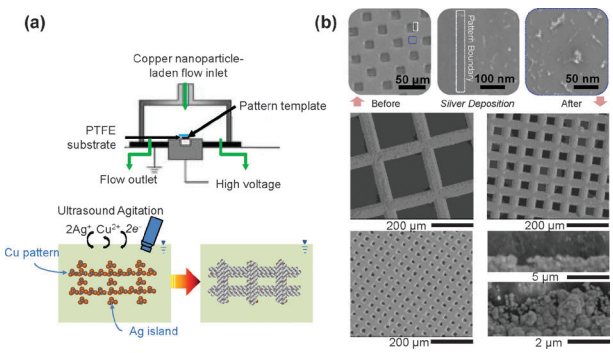

Fig. 4 Results for micropatterns of core–shell particles. (a) Schematic diagram of electrostatic patterning of the aerosol copper particles. (b) SEM images of the micropatterns before and after deposition of the silver.

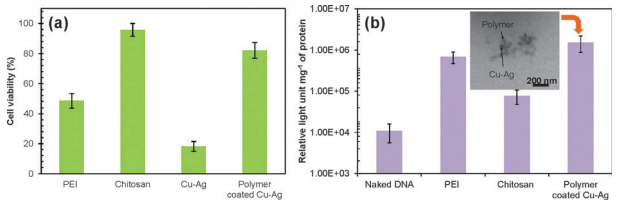

Fig. 5 *In vitro* measurements of (a) cell viability and (b) gene transfection efficiency for core–shell particles.

The average value of the resistivity of the pattern was approximately 9.8 μΩ cm, which is comparable to the theoretical resistivity of bulk silver (1.6 μΩ cm, *cf.* copper: 1.7 μΩ cm, nickel: 7.0 μΩ cm, iron: 10.0 μΩ cm).

We further tested the cytotoxicity and gene transfection properties of core–shell particles because inorganic nanoparticles are already interested in therapeutic and imaging applications.

Human embryonic kidney (HEK) 293 cells were incubated with core–shell particles for 24 h, and cell viability was determined through a standard MTT [3-(4,5-dimethylthiazol-2-yl)-diphenyltetrazolium bromide] assay (Fig. 5a). The results show that cell viability was ~18% for the particles, while the measured viabilities of the polyethyleneimine (PEI) and chitosan control systems were ~49% and ~96%, respectively. This implies that the particles were toxic that may not be suitable in a clinical context. Therefore, we employed a polymer mixture[13] to coat the core–shell particles by using the BR method,[14] and these particles were finally non-toxic (>82% in cell viability). We next examined the ability of the polymer coated particles (inset in Fig. 5b) to transfect HEK 293 cells using plasmid DNA that contain the luciferase and enhanced green fluorescent protein gene. The transfection efficiencies of particle–DNA complexes in the HEK 293 cell line were higher than those of naked DNA, PEI, and chitosan (Fig. 5b).

Herein we reported the development of copper–silver core–shell nanoparticles where aerosol copper nanoparticles served as the seeds for the continuous deposition of silver atoms on their surface. Initially copper nanoparticles were formed by spark discharge and then injected into the silver precursor solution in the presence of ultrasound to yield copper core–silver shell nanoparticles. This method was further employed to fabricate site selective silver deposition from the electrostatically patterned copper nanoparticles and to apply gene transfection as a polymer coated configuration for biomedical purposes. This method is new, simple, versatile, and environmentally friendly, and this or its modified version may be useful for other systems of nanoparticles for producing core–shell particles and patterns.

Experimental section

The PTFE substrate (11807-47-N, Sartorius, Germany) was used as a substrate for the copper particle deposits. A spark was formed between two identical copper rods (diameter: 3 mm; length: 100 mm; CU-112564, Nilaco, Japan) inside a chamber under a pure nitrogen environment (>99.99% purity) at standard temperature and pressure. The flow rate of the nitrogen gas was controlled by a mass flow controller (Tylan, US). The electrical circuit specifications were as follows: resistance 0.5 MΩ, capacitance 1.0 nF, loading current 1.1 mA, applied voltage 2.8 kV, and frequency 200 Hz.

The silver precursor solution was a mixture of solutions 1 and 2 at a 1 : 5 (v/v) ratio. 85 mg of silver nitrate (99.9%, Aldrich, US), used as a precursor of silver, was dissolved in 5 mL of deionized water (solution 1). 2 g of polyvinylpyrrolidone (M_w = 10 000, Aldrich, US), used as a protecting agent or stabilizing agent, was dissolved in 25 mL of ethylene glycol (99.9%, Aldrich, US) (solution 2).

The substrate was rinsed with deionized water after it was removed from the bath to remove the residual and then set aside to dry in a clean booth. Ultrasound (VCX 750, Sonics & Materials Inc., US) at 20 kHz (frequency) and 194.8 W cm^{-2} (ultrasound intensity) was applied into a solution for the silver deposition. The ultrasound was produced parallel to the liquid surface, and the copper deposited substrate was placed vertically.

A deposition density (D_d) of the substrate with aerosol copper nanoparticles is defined as follows:[15]

$$D_d(D_p) = Qt_dA_s^{-1}m^{-1}\int_0^{\infty}\eta(D_p)C_a(D_p)dD_p \qquad (5)$$

where Q is the flow rate of carrier gas, t_d is the deposition time, A_s is the plane area of substrate, $\eta(D_p)$ is the deposition efficiency (measured by SMPS before and after the deposition chamber), and $C_a(D_p)$ is the area concentration of the copper particles.

Notes and references

1 T.-H. Tran and T.-D. Nguyen, *Colloids Surf., B*, 2011, **88**, 1.
2 M. Tsuji, S. Hikino, R. Tanabe, M. Matsunaga and Y. Sano, *CrystEngComm*, 2010, **12**, 3900.
3 (*a*) K. J. Major, C. De and S. O. Obare, *Plasmonics*, 2009, **4**, 61; (*b*) L. Y. Chen, L. Zhang, T. Fujita and M. W. Chen, *J. Phys. Chem. C*, 2009, **113**, 14195; (*c*) S. E. Habas, H. Lee, V. Radmilovic, G. A. Somorjai and P. Yang, *Nat. Mater.*, 2007, **6**, 692.
4 M. Grouchko, A. Kamyshny and S. Magdassi, *J. Mater. Chem.*, 2009, **19**, 3057.
5 (*a*) M. Cazayous, C. Langlois, T. Oikkawa, C. Ricolleau and A. Sacuto, *Phys. Rev. B: Condens. Matter Mater. Phys.*, 2006, **73**, 113402; (*b*) M. Kahraman, Ö. Aydin and M. Çulha, *Plasmonics*, 2009, **4**, 293.
6 J. H. Byeon and Y.-W. Kim, *Ultrason. Sonochem.*, 2012, **19**, 209.
7 (*a*) J. H. Byeon, J. H. Park and J. Hwang, *J. Aerosol Sci.*, 2008, **39**, 888; (*b*) J. H. Byeon and J. T. Roberts, *ACS Appl. Mater. Interfaces*, 2012, **4**, 2515.
8 K. Ostrikov and A. B. Murphy, *J. Phys. D: Appl. Phys.*, 2007, **40**, 2223.
9 N. A. Fuchs, *The Mechanics of Aerosols*, Pergamon Press, Oxford, 1964.
10 S. Pyne, P. Sarkar, S. Basu, G. P. Sahoo, D. K. Bhui, H. Bar and A. Misra, *J. Nanopart. Res.*, 2011, **13**, 1759.
11 T. Som and B. Karmakar, *Nano Res.*, 2009, **2**, 607.
12 L. M. Dumitran, P. Atten, D. Blanchard and P. Notingher, *IEEE Trans. Ind. Appl.*, 2002, **38**, 852.
13 J. H. Byeon, H.-K. Kim and J. T. Roberts, *Macromol. Rapid Commun.*, DOI: 10.1002/marc.201200369.
14 J. H. Byeon and J. T. Roberts, *ACS Appl. Mater. Interfaces*, 2012, **4**, 2693.
15 (*a*) J. H. Byeon and J.-W. Kim, *Langmuir*, 2010, **26**, 11928; (*b*) J. H. Byeon and Y.-W. Kim, *ACS Appl. Mater. Interfaces*, 2011, **3**, 2912.